High membrane permeability for melatonin

Haijie Yu,[1] Eamonn J. Dickson,[1] Seung-Ryoung Jung,[1] Duk-Su Koh,[1,2] and Bertil Hille[1]

[1]Department of Physiology and Biophysics, University of Washington, Seattle, WA 98195
[2]Department of Physics, POSTECH, Pohang, Kyungbuk 790-784, Republic of Korea

The pineal gland, an endocrine organ in the brain, synthesizes and secretes the circulating night hormone melatonin throughout the night. The literature states that this hormone is secreted by simple diffusion across the pinealocyte plasma membrane, but a direct quantitative measurement of membrane permeability has not been made. Experiments were designed to compare the cell membrane permeability to three indoleamines: melatonin and its precursors N-acetylserotonin (NAS) and serotonin (5-HT). The three experimental approaches were (1) to measure the concentration of effluxing indoleamines amperometrically in the bath while cells were being dialyzed internally by a patch pipette, (2) to measure the rise of intracellular indoleamine fluorescence as the compound was perfused in the bath, and (3) to measure the rate of quenching of intracellular fura-2 dye fluorescence as indoleamines were perfused in the bath. These measures showed that permeabilities of melatonin and NAS are high (both are uncharged molecules), whereas that for 5-HT (mostly charged) is much lower. Comparisons were made with predictions of solubility-diffusion theory and compounds of known permeability, and a diffusion model was made to simulate all of the measurements. In short, extracellular melatonin equilibrates with the cytoplasm in 3.5 s, has a membrane permeability of ∼1.7 µm/s, and could not be retained in secretory vesicles. Thus, it and NAS will be "secreted" from pineal cells by membrane diffusion. Circumstances are suggested when 5-HT and possibly catecholamines may also appear in the extracellular space passively by membrane diffusion.

INTRODUCTION

This study concerns the ability of the pineal night hormone melatonin and its precursor N-acetylserotonin (NAS) to cross cell membranes. Melatonin and NAS are small indoleamines synthesized and secreted by the pineal gland throughout the night (Liu and Borjigin, 2006). Melatonin is recognized as a circulating hormone signifying night for both diurnal and nocturnal vertebrates (Reiter, 1991). It is synthesized only at night in two steps from serotonin (5-HT): (1) the N-acetylation of 5-HT produces NAS, and (2) the O-methylation of NAS produces melatonin (Fig. 1). Physiological interest in their membrane permeability lies in understanding the mechanism and speed of hormone secretion from pinealocytes. Could these small molecules be sufficiently impermeant to be stored sometimes in intracellular vesicles and secreted on demand by exocytosis, like the classical neurotransmitters acetylcholine and glutamate? Or are they so permeant that they always leave the cell by simple diffusion as fast as they are synthesized, like endocannabinoids and nitric oxide? The secretory mechanism determines the modes of physiological regulation. Exocytosis could be controlled by local calcium signaling acting on stored vesicles, whereas transmembrane diffusion would be regulated by the rates of synthesis.

A neurobiologist might assume that because melatonin and NAS are so closely derived from 5-HT, they would be secreted by exocytosis, as is known for 5-HT (Bruns and Jahn, 1995; Tao et al., 1997; Adell and Artigas, 1998). However, the N-acetyl moiety added to the free amine of 5-HT eliminates the protonation and charge of the amino group, so melatonin and NAS are uncharged. Furthermore, the neutral forms are relatively lipid soluble, and melatonin crosses the blood–brain barrier (van den Berg et al., 2004). Therefore, the pineal endocrine field concludes that the membrane permeability of melatonin is too high for anything but a passive mechanism of secretion (Simonneaux and Ribelayga, 2003), but there still have not been quantitative measures of membrane permeation. Here, we examine this concept by determining how fast these compounds can leave a cell. We extend the discussion to consider other amine neurotransmitters and drugs.

We compare the plasma membrane permeability of NAS and melatonin in living cells with that of 5-HT. We take advantage of the optical absorption, the fluorescence, and the oxidizability of indoleamines as well as the lipid solubility and known permeation of similar model compounds to estimate permeability coefficients. The conclusion is that melatonin and NAS have much

Correspondence to Bertil Hille: hille@uw.edu

Abbreviations used in this paper: 5-HT, serotonin; NAS, N-acetylserotonin.

higher membrane permeability than 5-HT and enter and leave cells in seconds. Thus, their secretion has to be regulated by their speed of synthesis.

MATERIALS AND METHODS

Cell culture and solutions

tsA201 cells were cultured in DMEM (Gibco) with 10% serum and 0.2% penicillin/streptomycin and passaged at 70% confluency. Pineal glands were obtained from male Sprague–Dawley rats (7–12 wk old) killed by CO_2 according to guidelines approved by the University of Washington Institutional Animal Care and Use Committee during the morning of their circadian light cycle. Glands were dissected into small pieces and digested with collagenase, and cells were triturated and cultured in fortified RPMI 1640 medium as described in Kim et al. (2008) and Yu et al. (2015). Cells were plated on poly-L-lysine–coated glass chips 12 h before experiments. For experiments, the extracellular saline solution contained (mM) 160 NaCl, 2.5 KCl, 2 CaCl$_2$, 1 MgCl$_2$, 10 D-glucose, and 10 HEPES, pH 7.3 adjusted with NaOH. The intracellular pipette solution for whole-cell dialysis of different indoleamines contained (mM) 130 KCl, 20 NaCl, 10 HEPES, 1 MgCl$_2$, 0.1 EGTA, 3 MgATP, and 0.3 Na$_2$GTP plus 10 indoleamine. For amperometric calibrations and photometric fluorescence measurements, extracellular solutions were exchanged within <1 s using a local perfusion system (Koh and Hille, 1997).

Because of potential degradation by oxidation, the indoleamine solutions were made fresh from powder every day at room temperature. 5-HT powder was added directly to the saline at 10 mM. At room temperature, melatonin is soluble in water to at least 20 mM (Shida et al., 1994). NAS and melatonin were first taken up in ethanol as a 400-mM stock and centrifuged and diluted into saline to make 10 mM. Neither the stocks nor the 10-mM mixtures showed any precipitate when centrifuged. In the experiments, the cells were exposed to the indoleamine bath

Figure 1. Chemical structures and enzymatic synthesis of melatonin from 5-HT. The AANAT (aralkylamine NAS) enzyme catalyzes the rate-limiting N-acetylation of 5-HT to give the intermediate NAS. The HIOMT enzyme methylates NAS to yield the hormone melatonin.

solutions for 20–30 s. Several control tests were performed with vehicle containing ethanol to be sure that the ethanol was not creating artifacts: there was no autofluorescence from the vehicle solution ($n = 4$); in cells perfused with 10 mM 5-HT in the bath, addition of the alcohol-containing vehicle induced no change of the isosbestic fluorescence of fura-2 inside cells ($n = 6$); in cells internally dialyzed with 10 mM 5-HT, perfusing the bath with the vehicle solution did not cause the appearance of an oxidation signal at an extracellular amperometric electrode ($n = 3$). These controls, which show that alcohol does not make the cell membrane more permeable to 5-HT, will become more understandable as similar experiments with melatonin are described in the Results.

Amperometric measurements

Carbon fiber microelectrodes were fabricated from 11-µm carbon fibers and 10 µl polypropylene micropipette tips (Koh and Hille, 1999). The insulating plastic layer covered the carbon fiber surface except near the tip where electric current is generated by oxidation of melatonin and its precursors. The electrode potential was 600 mV, allowing oxidation of 5-HT, NAS, and melatonin. Amperometric currents were recorded with an EPC-9 amplifier, filtered at 100 Hz, sampled at 500 Hz, and analyzed with IGOR Pro software (WaveMetrics). A second EPC9 amplifier was used when placing an on-cell or whole-cell dialysis patch pipette to monitor the seal resistance with the cell membrane. Cells were rejected if the seal resistance fell below 1 GΩ. When filled with the pipette solution, patch pipettes had a resistance of 3–5 MΩ. Recordings were performed at room temperature (22–24°C). The baselines of the raw amperometric records showed a slow decay representing very slow desensitization of the carbon fiber surface that was subtracted from the record by fitting an exponential curve to the baseline segments.

Photometric fluorescence measurements

Optical measurements of fluorescence from melatonin, NAS, 5-HT, and fura-2 were performed under an inverted microscope (Diaphot; Nikon). Cell monolayers or single cells were illuminated with a scanning monochromator light source (Polychrome IV; TILL Photonics), and the fluorescence was measured with TILL photodiodes using suitable filters and dichroic mirrors as described previously (Dickson et al., 2013). For indoleamines, the excitation wavelength was 358 nm and the fluorescence emission bandpass filter was 480/40 nm. For fura-2, the excitation wavelength was ∼370 nm, the isosbestic point of the dye, and the emission filter was 535/30 nm, leading to a second photodiode. The practical isosbestic setting of the scanning monochromator was determined by observing the crossover point of fura-2 emission changes while scanning the excitation between 340 and 400 nm before and after damaging the cell membrane in calcium-containing saline solution. Background fluorescence from areas without any cells was subtracted where indicated. The baseline autofluorescence of cells showed photobleaching and was corrected by subtracting a fitted exponential curve in Fig. 4. The fura-2 signals in Fig. 5 were corrected for photobleaching by fitting a falling exponential to the initial and final baseline segments and then dividing the whole sweep by the corresponding unitary exponential function. Error bars in Figs. 2 and 3 show SEM.

To study fura-2 fluorescence in the cytoplasm, cells were loaded with 2 µM fura-2-AM in saline solution supplemented with 0.2% Pluronic F-127 for 20 min. Cells were incubated in a dye-free solution for an additional 20 min to allow complete de-esterification of AM esters by endogenous esterases. Alternatively, the whole-cell pipette solution was supplemented with 100 µM fura-2 salt, and the cell was loaded by diffusion from the pipette.

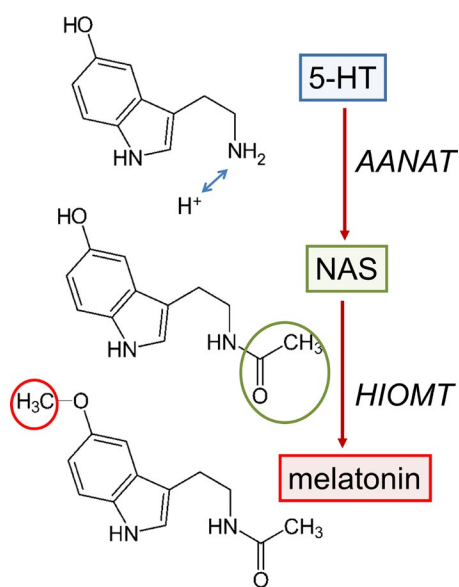Spectra of the indoleamines were measured with a DU 800 spectrophotometer (Beckman Coulter) for absorption spectra

and a Fluorolog Spectrofluorometer (Horiba Ltd) for emission spectra. Optical interaction of indoleamines with fura-2 was investigated on the epifluorescence microscope stage using 2-µl drops of mixtures covered with a coverslip and the same illuminator and optical detection as for the work with cells.

Mathematical modeling of membrane permeation and diffusion

A multicompartment diffusion model was made to simulate all the experiments. Finite difference equations representing the pipette, cell, and surrounding medium were solved in IGOR Pro testing different assumed indoleamine permeabilities of the cell membrane. The details are in the sections "A diffusion model of permeation by permeant compounds" and "Adding the pipette," and the program is in the supplemental text.

Online supplemental material

Fig. S1 and its legend show the absorption and emission spectra of indoleamines and how we chose the excitation and emission wavelengths for the experiments. The supplemental text, included in a separate TXT file, lists the IGOR Pro procedure used for simulating the diffusion of melatonin in the pipette, through the cytoplasm, across the cell membrane, and through the bath. Online supplemental material is available at http://www.jgp.org/cgi/content/full/jgp.201511526/DC1.

RESULTS

The structure of the paper is (a) to find several experimental measures of cell membrane permeability, (b) to compare the results with some molecules of known bilayer permeability, and (c) to develop a biophysical model that confirms the self-consistency of all these observations. To measure plasma membrane permeability, we asked how fast NAS and melatonin enter and leave cells, and we compared those results with similar experiments with 5-HT. We used four independent approaches.

Efflux is detected by amperometry

Our first method detects melatonin and NAS leaving the cells by amperometry. Like the catecholamines to which they are related, 5-HT, NAS, and melatonin can be measured amperometrically by the oxidative removal of electrons at a positive electrode. Our experimental approach started with the tsA201 cell line as a model cell and detection of indoleamines extracellularly by their oxidation current using a micro carbon fiber electrode held in the bath almost touching the cell surface. As Fig. 2 A shows, we tested the indoleamines by adding them to patch pipette solutions and sealing the pipettes onto cells; at the same time, we probed the extracellular solution for amperometric signals from oxidizable compounds diffusing out of the cell. In the cell-attached configuration and especially after breaking through to whole-cell configuration, the indoleamine in the pipette solution might enter the cytoplasm and diffuse to the extracellular space if it is membrane permeant. In Fig. 2 B the whole-cell pipette includes 10 mM melatonin, a high amount needed to produce readily resolved currents outside the cell. The amperometric current trace shows three deflections as the carbon fiber electrode is advanced and withdrawn three times (arrows) from nearly touching the cell surface. It is clear from the current deflections that oxidizable substrate is present in the extracellular medium close to the cell. The experiments were repeated with NAS and 5-HT (Figs. 2, C and D), giving noticeably smaller oxidation signals for NAS and only marginally detectable ones (sometimes) for 5-HT. The 5-HT trace shown in the figure is the largest of those recorded with this compound, and we are not confident that it represents a real 5-HT signal. Melatonin and NAS clearly do escape from the cell.

How much indoleamine is escaping? The carbon fiber electrode was calibrated by recording its responses to known indoleamine concentrations perfused rapidly by its active tip. This gave three linear concentration–response relations with different slopes (Fig. 2 E). 5-HT solutions were oxidized the most efficiently. At a 600-mV electrode potential, the slopes for melatonin, NAS, and 5-HT currents were 4.99 ± 0.07 ($n = 4$–10), 2.97 ± 0.07 ($n = 3$–10), and 20.6 ± 0.2 µA/µM ($n = 4$–8). From this calibration, the mean amperometric deflections for efflux experiments like those of Fig. 2 (B–D) could be translated into apparent surface concentrations close to the cell (Fig. 2 F). With 10 mM melatonin in the whole-cell pipette, the detected extracellular concentration near the cell was 2.8 ± 0.3 µM. (Quantitative results like these are accumulated in Table 1 for later comparison with quantitative modeling.) The estimated extracellular concentrations for melatonin, NAS, and 5-HT were in the ratio 1:0.18:0.006 (actual values: 2.8 ± 0.3 [$n = 6$], 0.50 ± 0.02 [$n = 11$], and 0.020 ± 0.001 µM [$n = 17$]), providing a preliminary sequence of cell membrane permeabilities for these indoleamines at pH 7.4: melatonin > NAS >> 5-HT. For 5-HT, we regard the 0.006 value as just an upper limit.

Further control experiments showed that the amperometric signals behaved as expected and were almost identical when pinealocytes were used instead of tsA201 cells. As schematized in Fig. 3 A, the extracellular solution was probed to monitor the spatial extent of the spread of indoleamine outside the cell. As the carbon fiber was moved in successive 30-µm steps away from the cell, deflections for melatonin fell off progressively with distance (Fig. 3 [B and C] for tsA201 cells). Small extracellular signals were actually present even with the on-cell configuration of the melatonin pipette (Fig. 3 B), but they became fivefold larger after breakthrough to whole-cell configuration (Fig. 3 C). Fig. 3 D shows a similar experiment in a representative pinealocyte. It starts in on-cell configuration, measuring three times, breaks through to whole-cell configuration, and then, after three measurements at the cell surface, probes the extracellular space in 30-µm increments.
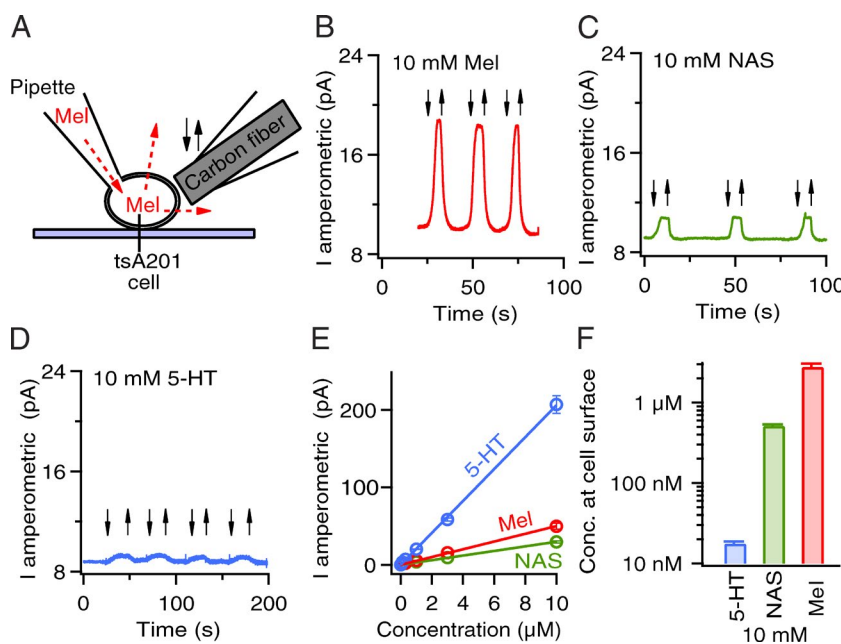
Figure 2. Amperometric detection of indoleamine leakage from a tsA201 cell. (A) Schematic showing whole-cell pipette with melatonin (Mel) and a carbon fiber amperometric electrode in the bath. (B) Amperometric oxidation currents seen as the carbon fiber electrode in the bath are advanced to almost touch the cell (down arrows) and then pulled away (up arrows) three times (representative trace). (C and D) Same as in A and B but for whole-cell pipettes containing NAS or 5-HT. For 5-HT, the trace shown is the one with the largest oxidation signal. (E) Calibration curves showing the carbon fiber sensitivity to flowing indoleamine solutions of known concentration ($n = 4$–5). (F) Estimated mean bath concentration (conc.) of indoleamine near the cell surface for experiments like B–D. Note the semilogarithmic axes ($n = 5$–10). Error bars show SEM.

The extracellular signals were indistinguishable between tsA201 and pineal cells, and they fell off with distance in the same way with either cell type and with either pipette configuration (Fig. 3 E). Fitted empirically as an exponential fall off in space, the approximate space constant of decay was 30 ± 2 µm ($n = 5$) in the bath for tsA201 cells and 32 ± 4 µm ($n = 7$) for pinealocytes. The finding that extracellular melatonin was readily detected even in the on-cell pipette configuration shows that the membrane offers only a modest barrier to melatonin diffusion. In on-cell mode, the compound would have to diffuse through two membranes, first a small patch of membrane in the on-cell pipette and then the large cell membrane around the whole cell. Later in this paper, the amperometric measurements are used to develop a quantitative interpretation. But already they provide our first evidence of membrane permeability for melatonin and NAS that is significantly higher than that for 5-HT. They also indicate that the tsA201 cell is an appropriate model for pinealocytes with respect to passive membrane permeation to indoleamines. From this point on, all experiments were performed with tsA201 cells.

Influx and efflux detected by in-cell fluorescence

Our second approach monitors penetration of melatonin by its fluorescence. Like tryptophan from which they derive, the indoleamines absorb light in the UV and emit fluorescence in the blue-visible spectrum. Fig. S1 documents some spectral properties, and its legend describes the choice of excitation and emission wavelengths for our experiments. The strategy of the experiments was to observe fluorescence transients as extracellular indoleamine (10 mM) was perfused in a step pulse through the microscope chamber, comparing the results with and without a monolayer of cells in the field of view (Fig. 4 A). To understand the results, we first consider idealized experiments. Without cells, the fluorescence emission signal should show a large step up and down with kinetics, reflecting only the rapid kinetics of perfusion of the fluorescent molecule (Fig. 4 B, top black). With cells present, the result would be

TABLE 1
Comparison of tsA201 experiments and simulations

Property	Experiment	Model
Pipette resistance (MΩ)	3–5	4.4
Plasma membrane area (pF//µm²)	20//2,000	8.0//804
Diffusion coefficient melatonin (cm²/s)	6×10^{-6a}	6×10^{-6}
Cell-bath equilibration time constant for melatonin (s)	3.5	3.54
Membrane permeability melatonin (µm/s)	-	1.7
Exponential melatonin space constant outside cell (µm)	30	22
Extracellular concentration with 10 mM melatonin in the whole-cell pipette (µM)	2.8	11.6
Extracellular concentration with 10 mM melatonin in the on-cell pipette (µM)	0.56	2.3

[a]Rice et al. (1985).

slightly more complex. There would be an excluded volume (the cells) so that the fluorescence step from the reduced solution space would not quite be as high (Fig. 4 B, top red). But if the indoleamine is permeant, the fluorescence should then creep up gradually to the full level with kinetics that reflect the penetration and filling of the cell volume (Fig. 4 B, top blue). Subtraction of the record without cells from that with cells (giving ΔF) would reveal a transient filling and emptying of the cell volume if the indoleamine is permeant (Fig. 4 B, bottom). In this idealized example, the initial down step of the ΔF trace is 20% of the full unsubtracted, no-cell step because the thickness of the cell monolayer was assumed to occupy 20% of the objective's light-gathering depth of field in the perfusion chamber.

Fig. 4 C shows actual experiments. Without cells (five superimposed black traces), melatonin and 5-HT perfusion result in quick, reversible rises of fluorescence. (These and all traces are already corrected for photobleaching; see Materials and methods.) They show that with our microscope filters, the fluorescence emission of 5-HT is about seven times that of the same concentration of melatonin. Then, with a monolayer of tsA201 cells (five violet traces), there is a background of fluorescence even before perfusion of compounds because the cells are autofluorescent between 400 and 500 nm. The transient properties during perfusion steps are best seen in the mean difference trace ΔF in Fig. 4 D. Here, the monolayer autofluorescence has been subtracted already so the mean difference trace is centered at zero. Looking first at the 5-HT application and comparing it with the idealized ΔF traces in Fig. 4 B (bottom) reveals that 5-HT behaves as an impermeant molecule on this time scale. There is neither a transient increase after the on step nor a transient decrease after the off step. The initial down step and the later up step of the ΔF trace are 8–10% ($n = 6$) of the full 5-HT, no cell step. Presumably, the cell monolayer thickness occupies the equivalent of ∼9% of the light-collecting depth of field of the objective.

In contrast, melatonin behaves as a permeant compound in this assay, with transient changes after the on step and the off step. However, they do not have exactly the configuration of the idealized traces in Fig. 4 B (bottom). The mean of the initial down step and the later up step of the trace is again roughly 9%, but unexpectedly, while melatonin is putatively diffusing into the cell (between the 20- and 40-s time points), the total light quickly rises above the level seen with no cells. We offer two nonexclusive explanations for this overshoot. One hypothesis is that the excess signal reflects the lipid solubility of melatonin. Not only does it enter cells by diffusion but it also accumulates in all of the internal membranes of the cells and at any other hydrophobic sites. Thus, the fluorescence overshoot could indicate that cells accumulate a reservoir of excess melatonin,

passively as an internal "bound pool." A second hypothesis described in the section on modeling is that melatonin has a higher fluorescence quantum yield in the environment of the cytoplasm. Fitted with a single exponential, the time constant of the rise of fluorescence here is ∼3.5 s and that of the later fall is ∼7 s. This would be the lumped time constant of entry and any hydrophobic accumulation. Again, in this second type of measurement, melatonin is membrane permeant and 5-HT is not. NAS could not be tested because we could not excite NAS fluorescence with our optics.

Influx and efflux detected by quenching

Our third type of measurement involves optical quenching. Because indoleamines absorb light, they show optical
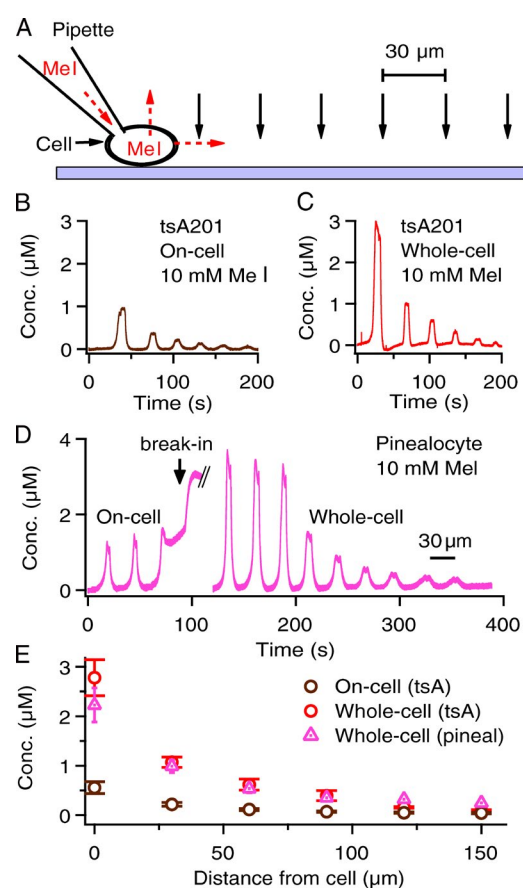

Figure 3. Spatial decay of the amperometric signal with melatonin. (A) Schematic of spatial measurements of melatonin (Mel) diffusion from a cell with successive carbon fiber placements (arrows) at 30-µm increments from the cell. (B) Results of an experiment with the melatonin pipette patched on a tsA201 cell before breakthrough. (C) A different tsA201 cell after breakthrough to whole-cell configuration. (D) The same kind of experiment as in B and C with a rat pinealocyte showing the transition from on-cell to whole-cell recording. Again, the carbon fiber is brought to the cell surface three times with each configuration, and then it is moved to points successively 30 µm away. (E) Mean spatial concentration profiles for on-cell and whole-cell experiments with tsA201 and pineal cells ($n = 5$–6). Error bars show SEM.

interactions when mixed with other fluorescent molecules. Thus, with fluorometer measurements, we found that in calcium-free mixtures, indoleamines decreased the fluorescence of the calcium-sensitive dye fura-2. When 10 mM indoleamine was mixed into 100 µM fura-2 in a coverslip experiment on the microscope stage, the fura-2 fluorescence fell to 82 ± 1% ($n = 6$), 73 ± 1% ($n = 6$), and 46 ± 1% ($n = 6$) by additions of NAS, melatonin, and 5-HT, respectively. This might be quenching by fluorescence resonance energy transfer or by collisions or perhaps an inner-filter effect (Sharma and Schulman, 1999). We reasoned therefore that if we preloaded a cell with fura-2 and exposed it to indoleamines in the bath, we might be able to observe penetration of the indoleamine as a gradual dimming of the intracellular fura-2 fluorescence (Fig. 5 A). In these experiments, fura-2 was excited at its empirical isosbestic point, 370 nm (see Materials and methods), so its fluorescence was not calcium sensitive, and the fura-2 fluorescence was recorded between 505 and 565 nm. Fig. 5 B shows the processed (see legend) result of such experiments using single fura-2-AM–loaded cells. Bath melatonin decreases the fluorescence of fura-2 inside the cells (by 14%), but 5-HT does not (<0.5%). The rise of the melatonin effect has a time constant of 4.9 ± 0.3 s ($n = 14$), and the fall has one of 3.5 ± 0.1 s ($n = 14$). Similar experiments were performed on cells dialyzed with 100 µM fura-2 salt by a whole-cell pipette. Again fura-2 fluorescence is decreased 14% by melatonin and not by 5-HT. For melatonin, the mean time constant for onset is 3.3 ± 0.3 s ($n = 5$), and that for offset is 4.2 ± 0.5 s ($n = 5$). In separate experiments with applications of NAS, the fluorescence was slightly increased, an optical effect that we do not understand now. Independent of the previous two approaches, the fura-2–quenching

assay shows again that melatonin permeates and escapes cells within a few seconds, and 5-HT is not measurably permeant.

Comparison of indoleamines with other model compounds

For our fourth completely independent approach to estimating membrane permeability, we compare physical properties of indoleamines with those of model compounds. Table 2 lists several small compounds sorted in order of increasing n-octanol/water partition coefficient of their uncharged species, K_{oct}. Among them, the partition coefficients for indoleamines rise in the order 5-HT < NAS < melatonin as more carbons are added to the structure and the polar amine and hydroxyl are masked (Fig. 1). K_{oct} values of 4.8 and 25 for NAS and melatonin mean that their equilibrium concentrations in n-octanol would be 4.8 and 25 times that in water, respectively. As is explained in the Appendix, according to the solubility-diffusion theory (Finkelstein, 1976; Orbach and Finkelstein, 1980), the membrane permeability of such small molecules should be closely correlated with their lipid solubility. The precise definition of the permeability coefficient P and its units are given by Eq. 4 in the Appendix and the discussion there. Table 2 gives a few measured membrane permeability coefficients (of neutral species) measured in various planar lipid bilayers. Four can be compared because they are for similar bilayers made from egg lecithin/hexadecane or phosphatidylcholine/decane (Finkelstein, 1976; Orbach and Finkelstein, 1980). They correlate with octanol partition coefficients as shown by red circles in Fig. 6. These measured values allow us to predict lecithin membrane permeabilities for the other compounds in Table 2 (Fig. 6, top red crosses and red line). The predicated lecithin planar bilayer permeability for melatonin is
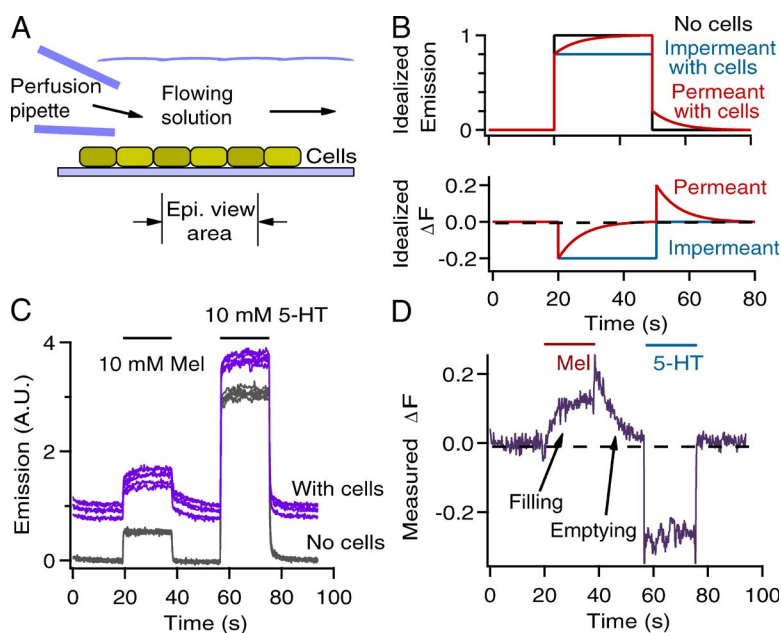
Figure 4. Comparing melatonin and 5-HT permeation using their fluorescence. (A) Schematic showing a monolayer of tsA201 cells on a coverslip locally perfused by a pipette containing control saline or saline supplemented by 10 mM melatonin (Mel) or 5-HT. The epi-illumination and fluorescence recordings use a 40× objective below the coverslip in a circular field of view of 39 µm that is several cell diameters wide. (B, top) Three idealized fluorescence recordings for a step pulse of perfusion with three conditions: no cells, with cells and an impermeant indoleamine, and with cells and a permeant indoleamine. (bottom) Idealized fluorescence difference traces ΔF of a record with cells minus a record without cells (see section "Influx and efflux detected by in-cell fluorescence"). (C) Five superimposed fluorescence traces from five chips without cells (gray) and from five chips with cells (purple) as melatonin and 5-HT are locally perfused for 20 s. (D) Mean difference fluorescence ΔF for the experiment in C; mean data with "No cells" are subtracted from mean data "With cells."

2,250 µm/s. A fifth measured compound, indole-3-ethanol, was studied in rather different planar bilayers made with a mixture of tocopherol/cholesterol and brain lipids (Bean et al., 1968). This measurement is plotted as a red triangle near the bottom of the graph (Fig. 6). Clearly, sterol-containing bilayers are far less permeable than lecithin ones. The Appendix gives arguments why plasma membranes might also have membrane permeability values several orders of magnitude lower than those for lecithin planar bilayers, including this effect of sterol lipids. We return later to the bottom set of green symbols in Fig. 6, which represent our educated guess for permeabilities in plasma membranes.

A diffusion model of permeation by permeant compounds

We now have three types of experiments as well as comparisons with model compounds to estimate membrane permeability. To synthesize a self-consistent conclusion, we made a diffusion model with the goal of replicating all of the data summarized in Table 1. The objective was to gain confidence in each type of observation and to converge on membrane permeability values for the indoleamines. The presentation now becomes more biophysical. For mathematical simulations, the cell (8-µm radius) and its surroundings were represented as a simple nested set of thin spherical shells of thickness $\Delta x = 0.5$ µm (Fig. 7 A) with fluxes between them that obeyed either Fick's law of diffusion, $-DA\,\Delta c/\Delta x$, where D is the diffusion coefficient, or, when at the cell membrane, the familiar membrane permeation equation, $-P_m A\,\Delta c$. The free diffusion coefficient for melatonin was taken as 0.6×10^{-5} cm^2/s, like those reported for epinephrine, dopamine, and 5-HT (Rice et al., 1985). These finite difference equations were integrated in time steps of 40 µs by the simple first-order Euler method. The code for the simulation is given in the Supplemental material as an IGOR Pro procedure (supplemental text).

First, we had to address the unexpected observation in Fig. 4 D. There, the subtracted fluorescence transients revealed that melatonin fluorescence rose above the bath value when a cell was present. In the model, we interpret this as indicating that melatonin accumulates in cells above the ambient concentration in the bath. Therefore, we included in our model the equivalent of a cellular hydrophobic phase that would create a "bound" or adsorbed pool of melatonin in the cytoplasm that was assumed to be in instantaneous equilibrium with the free cytoplasmic pool. After trials, the bound pool in the cell was set at 1.2 times the free pool, making a total fluorescence 2.2 times that expected had there been no bound pool. We propose that this represents interaction of highly lipid-soluble melatonin with cellular hydrophobic sites, including intracellular membranes. Our assumption is strikingly similar to a model developed for kinetics of phenobarbital action on intact cells (Gingrich et al., 2009). There, the time course of

the hydrophobic drug ($K_{oct} = 108$) at the external cell surface during bath application and removal was modeled to include the cellular membranes as a hydrophobic "pharmacodynamic compartment." In that paper, the entire cell, including its internal membranes, was treated as a single hydrophobic compartment. This compartment bound 108*0.14 or 15 U phenobarbital, which was released on washout with a time constant of 4.3 s. A different interpretation of the excess fluorescence we saw would be that in the intracellular environment the quantum efficiency of melatonin fluorescence is elevated to 2.2-fold that in the bath. Indeed, quantum yield for some fluorophores can be elevated in solvents of higher viscosity (Haidekker et al., 2005), and the cytoplasm does have a 20–40% elevated viscosity relative to extracellular saline (Fushimi and Verkman, 1991).

Next, we considered the time constant for filling and emptying of the cell, the parameter that is most directly indicative of the membrane permeability. In our fluorescence experiments, melatonin time constants ranged from 3 to 7 s with a median at 3.5 s (Figs. 4 D and 5 B).
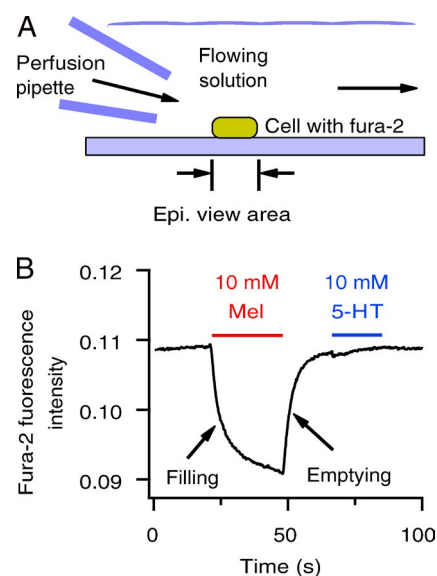

Figure 5. Comparing melatonin and 5-HT permeation using quenching of an intracellular fluorescent dye. (A) Schematic of a single cell on a coverslip locally perfused by a pipette containing control Ringer or Ringer supplemented by 10 mM melatonin (Mel) or 5-HT. The epi-illumination and fluorescence recordings use a 40× objective below the coverslip with a rectangular field of view stopped down to include just the one cell. (B) Mean fluorescence of fura-2-AM–loaded single cells as indoleamine solutions are perfused rapidly. The trace in B is derived from original records as follows. Separate single-cell fluorescence traces for 14 perfused coverslips were averaged and corrected for photobleaching. Traces for 12 perfused cell-free areas were treated similarly and subtracted from the with cell traces to correct for a small additional fluorescence contributed by the indoleamine compounds applied in the bath. This correction subtracted a step of fluorescence of 0.5×10^{-3} from the melatonin period and of 4.6×10^{-3} from the 5-HT period. Excitation wavelength was 370 nm.

Our model will replicate cell-filling and cell-emptying time constants of 3.5 s if we set the "melatonin" membrane permeability coefficient to 1.7 µm/s (Table 1). The resulting model outputs are shown in Fig. 7 (B and C) as simulations of the kinetic experiments of Figs. 4 D and 5 B. They have appropriate time constants. Fig. 7 B also shows an overaccumulation of melatonin in the cell, as was seen in the fluorescence experiment of Fig. 4 D. The extent of intracellular binding of melatonin was chosen to fit this experiment. Fig. 7 C includes two additional simulations with slower and faster relaxations resulting from assuming a membrane permeability that is 0.2 or 5 times 1.7 µm/s. As anticipated, these traces show time constants that are almost exactly fivefold larger ($\tau = 17.3$ s) and smaller ($\tau = 0.77$ s) than for the standard membrane permeability ($\tau = 3.54$ s). It is clear that permeability values can be chosen with some confidence from the experimental time constants.

Adding the pipette

Finally, the whole-cell pipette could be added to the model. Fig. 7 D shows its assumed geometry, a 10-µm radius at the large end, tapering continuously to 0.98-µm radius, and then dropping abruptly to a final 0.3-µm radius for the last 0.5 µm. The vertical tick marks along the pipette walls mark the position of each 0.5-µm planar

slice in the simulation geometry. The tip dimensions were chosen to give the pipette an integral resistance of 4.4 MΩ, including the external access resistance (assuming a resistivity of 80 Ω cm for the filling solution). To maintain a symmetry in the model that simplified its formulation, the pipette tip was connected to the central smallest spherical shell of the cell cytoplasm. Concentration gradients within the cytoplasm were negligible, so there was little error from not placing the simulated pipette at the cell surface. Thus, the diffusion regimen has the configuration shown schematically in Fig. 7 E, pipette, cell, membrane, and external unstirred layer. The pipette tip and the membrane are expected to be the two rate-limiting barriers.

Now we can "fill" the whole-cell pipette with 10 mM "melatonin" and simulate the diffusion processes of the amperometry experiments of Fig. 3. The calculated concentration profile after 30 s of integration is shown in Fig. 7 F using the chosen membrane permeability at the cell surface. The distance scale starts with 50 µm of pipette at the left, 8 µm of cytoplasm, and then 142 µm of bath at the right, and the pipette is the source of melatonin. Melatonin is high in the wide part of the pipette (clamped at the wide end), falling off abruptly in the last narrowest segment of the tip (see two isolated black symbols there), falling gently across the cytoplasm,

TABLE 2

Physical properties of permeant and "impermeant" compounds

Compound	MM	Chemical formula	pK$_a$ and pK$_b$	% neutral at pH 7.4	log K$_{oct}$[a]	K$_{oct}$ neutral	K$_{oct}$ * % neutral/100	P$_{measured}$[b] neutral	P$_{cell}$[c] at pH 7.4	τ[d] 16-µm diameter cell
	D			%				µm/s	µm/s	
Norepinephrine	169.2	C$_8$H$_{11}$NO$_3$	8.6	6	−1.11	0.078	0.005	-	0.0003	5.1 h
Epinephrine	183.2	C$_9$H$_{13}$NO$_3$	8.6	6	−0.87	0.13	0.008	-	0.0006	2.9 h
1,4-Butanediol	90.1	C$_4$H$_{10}$O$_2$	>15	100	−0.70	0.20	0.20	3[e]	0.014	7.2 min
Nitric oxide	30.0	NO	−2.9	100	−0.35	0.45	0.45	-	0.031	3.2 min
5-HT	276.2	C$_{10}$H$_{12}$N$_2$O	9.7	0.50	0.50	3.2	0.016	-	0.0011	1.5 h
Butyric acid	88.1	C$_4$H$_8$O$_2$	4.7	0.2	0.70	5.0	0.01	1,000[e]	0.3	17 s
NAS	218.3	C$_{12}$H$_{14}$N$_2$O$_2$	10.1	99.8	0.68	4.8	4.8	-	0.3	18 s
Nicotine	162.2	C$_{10}$H$_{14}$N$_2$	8.0	20	1.10	12.6	2.5	-	0.2	34 s
Codeine	299.4	C$_{18}$H$_{21}$NO$_3$	9.7	0.50	1.24	17	0.09	1,400[e]	0.006	16 min
Melatonin	232.3	C$_{13}$H$_{16}$N$_2$O$_2$	16.3	100	1.39	25	25	1.7[f]	1.7	3.5 s
Indole-3-ethanol[g]	161.2	C$_{10}$H$_{11}$NO	15.2	100	1.62	42	42	2.3[h]	2.9	2.1 s
Hexanoic acid	116.2	C$_6$H$_{12}$O$_2$	4.8	100	1.71	51	51	11,000[i]	3.6	1.7
Lidocaine	234.3	C$_{14}$H$_{22}$N$_2$O	7.9	24	2.15	141	33.9	-	2.4	2.5 s

MM, molecular mass; pK$_a$ and pK$_b$, acid or base equilibrium dissociation constant; log K_{oct}, logarithm to base 10 of *n*-octanol/water partition coefficient of neutral form; K_{oct}, partition coefficient of neutral form.

[a]Each log K_{oct} value is the mean of several calculated and experimental "logP" values reported in the DrugBank database (Law et al., 2014) and the SciFinder database of the American Chemical Society. K_{oct} is computed from these mean values. See also discussion in Sangster (1989).

[b]$P_{measured}$, experimental membrane permeabilities measured in planar lecithin bilayers or in tsA201 cells.

[c]P_{cell}, predicted permeabilities for cell membranes at pH 7.4 calculated from Eq. 1b.

[d]τ, predicted exponential equilibration time constant between inside of cell and bath at pH 7.4 calculated from Eq. 2 for a 16-µm diameter cell.

[e]Three values of membrane permeability measured experimentally with egg lecithin/hexadecane painted planar lipid bilayers (Finkelstein, 1976; Orbach and Finkelstein, 1980).

[f]P_m in tsA201 cells from this paper.

[g]Also called tryptophol.

[h]Membrane permeability measured experimentally with tocopherol/cholesterol/brain phospholipid/chloroform-methanol painted planar lipid bilayers (Bean et al., 1968).

[i]Membrane permeability measured experimentally with egg phosphatidylcholine/decane painted planar lipid bilayers (Walter and Gutknecht, 1986).

dropping abruptly one more time across the membrane, and then decaying away in the bath. This is the expected downhill cascade crossing two major barriers.

We compare these simulations with the amperometric experiments of Figs. 2 and 3. The experiments detected 2.8 µM melatonin in the bath near to the cell when the whole-cell pipette contained 10 mM melatonin and a fivefold smaller value when the pipette was in on-cell configuration (Table 1). The simulation predicts 11.6 µM extracellular melatonin close to the cell for whole-cell dialysis and a fivefold smaller value for on-cell configuration versus whole-cell dialysis (Fig. 7 F, red trace). The agreement of the fivefold drop for on-cell configuration was not an independent prediction. It was achieved by manipulating a parameter, adjusting an enlarged membrane area for an Ω-shaped on-cell membrane patch in the pipette tip (see red dashed line in Fig. 7 D and figure legend). The augmented area is not outside of normal experience.

We can consider several reasons why the experimentally detected extracellular concentrations might be artifactually lower than predicted by the model. (a) The carbon fiber electrode is not a simple right cylinder insulated to the tip. The insulation reaches irregularly to within several micrometers of the tip, and the tip itself is a jagged fractured end of the fiber (Koh and Hille, 1999). Therefore, when the tip is very close to the cell, it must be averaging concentrations over at least a 5-µm range away from the cell. For this reason, we actually quote calculated values at 2.5 µm from the membrane shell in this paper. However, the gradient of concentration is really not steep enough for this to be a large factor. (b) The amperometric oxidation might be consuming a significant fraction of the melatonin coming out of the cell, a situation not represented in the simulation. We can calculate how much is consumed. In the case of Fig. 7 F (whole cell), the steady state cytoplasmic concentration is 0.77 mM and the membrane area is 804 µm^2, giving (with $P_m = 1.7$ µm/s) a net efflux from the cell of 1.10^{-15} mol/s or 660×10^6 molecules/s. During the experiment, the carbon fiber is passing ∼9 pA (Fig. 2 B), which at 1.6×10^{-19} C/electron corresponds to 56×10^6 electrons/s. The oxidation requires two electrons per molecule, so only ∼4% of the total number of emerging melatonin molecules are being consumed by the oxidation. (c) Carbon fiber electrodes respond better to fast-flowing solutions than to stationary ones. When solution flow is stopped, the reading sags as local depletion develops in an unstirred layer closely adjacent to the carbon fiber surface ("electrode polarization"). Our carbon fiber calibration used fast-flowing solutions, whereas the measurements around the cell used stationary solutions. In the end, although it gives the right orders of magnitude, we do not clearly establish why our simulation predicts four times more extracellular melatonin than we see with the amperometric electrode.

The concept of local unstirred layers and electrode polarization may have the most merit.

The calculation of Fig. 7 F gives another measured quantity, the spread of melatonin away from the cell surface. As the figure shows, the spatial profile is not exactly an exponential one. Nevertheless, fitting an exponential starting 20 µm away from the cell gives a space constant of ∼22 µm from the model compared with 30 µm from the tsA201 cell experiments of Fig. 3. The decay comes from diffusion into the ever-expanding volumes of successive spherical shells.

In short, and neglecting small deviations, the model simulations show a broad self-consistency of the three classes of experimental measurements that we presented. All of the observations and the modeling support a high membrane permeability for melatonin in the range of a few micrometers per second and a diffusional equilibration time of a few seconds between bath and cell.

Spatial profiles of permeant molecules

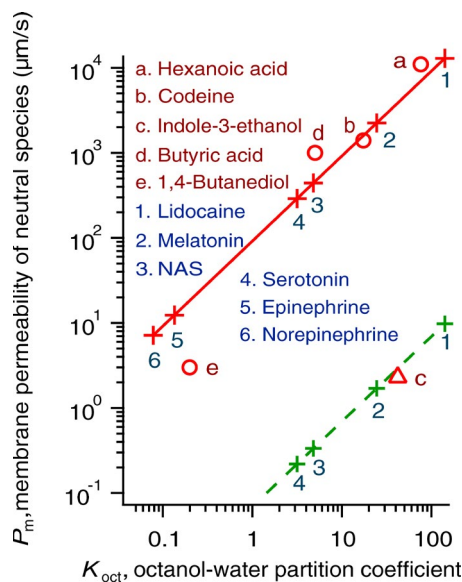In Fig. 7 F, we saw a cascade of diffusion down a monotonically falling concentration gradient. Much of this

Figure 6. Membrane permeabilities for uncharged species plotted against *n*-octanol/water partition coefficients for indoleamines and model compounds. Compounds and partition coefficients are from Table 2. Red circles are measurements from Orbach and Finkelstein (1980) fitted with a unity slope regression line (Eq. 3). Red crosses are compounds of physiological interest, including indoleamines predicted using Eq. 3 for lecithin membranes and assuming that they are in a 100% uncharged form. The red triangle below is indole-3-ethanol from Bean et al. (1968) measured in tocopherol/cholesterol/brain lipid membranes. Green crosses below include the indoleamines, plotted with Eq. 1a, which gives permeabilities 1,322-fold lower than Eq. 3. The green relationship is our best guess for biological membranes using P_{cell} for melatonin set at 1.7 µm/s. Note that for all compounds that protonate, the practical permeability will be lowered further as a function of pH because the charged forms are nearly impermeant. Such reduced values are given as P_{cell} in Table 2 and Eq. 1b for pH 7.4.

profile would be inaccessible to normal experimentation, so several informative lessons can be drawn from the simulations. The results remind us that in dialysis experiments with a permeant molecule, the concentration in the cytoplasm never reaches that in the whole-cell pipette. In this example, the predicted steady state concentration in cytoplasm is only 0.77 mM, although there is 10 mM melatonin in the whole-cell pipette. Furthermore, because fewer molecules are needed to attain the low steady state cytoplasmic concentration, the time constant for the cell to approach steady state with the whole-cell pipette is faster (3.5 s), just as it was for diffusional entry from the bath (Fig. 7 C). If instead, we made the test molecule impermeant and without a cytoplasmic bound pool, like for example fura-2 dye, this pipette and cell combination predicts a pipette–cytoplasm equilibrium time constant of 20 s, and if the melatonin-binding process is restored, it lengthens to 42 s. However, in our case, a significant melatonin membrane permeability makes it much shorter.

It is instructive to consider the effects of membrane permeability on the diffusion profile as shown in Fig. 7 G. Here the standard 1.7-μm/s permeability for melatonin has been increased and decreased by factors of 10 and 100. Not surprisingly, when permeability is decreased, less of the diffusing molecule appears in the bath, and more of it stays in the cytoplasm. The membrane barrier becomes high in the schematic of Fig. 7 E. At low enough P_m, the extracellular concentration becomes linearly proportional to the P_m value, the intuitive result. Note that the concentration traces cross over at the membrane and so have the opposite order in the extracellular medium as in the cell. (Not shown is that the time constant for pipette equilibration with the cytoplasm is increasing as well.) Interestingly, when the permeability is increased instead, there is very little gain in efflux. The membrane barrier in Fig. 7 E becomes very low. The three extracellular traces for $1 \times P$, $10 \times P$, and $100 \times P$ are nearly superimposed, and we approach the point where the permeability is so high that it is almost as if the membrane were not there, and the spread is governed only by continuous free diffusion through the cytoplasm and bath. The one remaining rate-limiting step is the escape of molecules through the narrow tip of the pipette unopposed by return from the cytoplasm into the pipette. That sets the efflux from the cell.

DISCUSSION

Consequences for experimental physiology

Our results accord fully with the conclusion in the pineal field that melatonin is sufficiently lipid soluble to leave the pinealocyte without a special secretory mechanism (Simonneaux and Ribelayga, 2003). Now we understand this quantitatively. We have shown that the sojourn of melatonin in a tsA201 cell is only 3–4 s
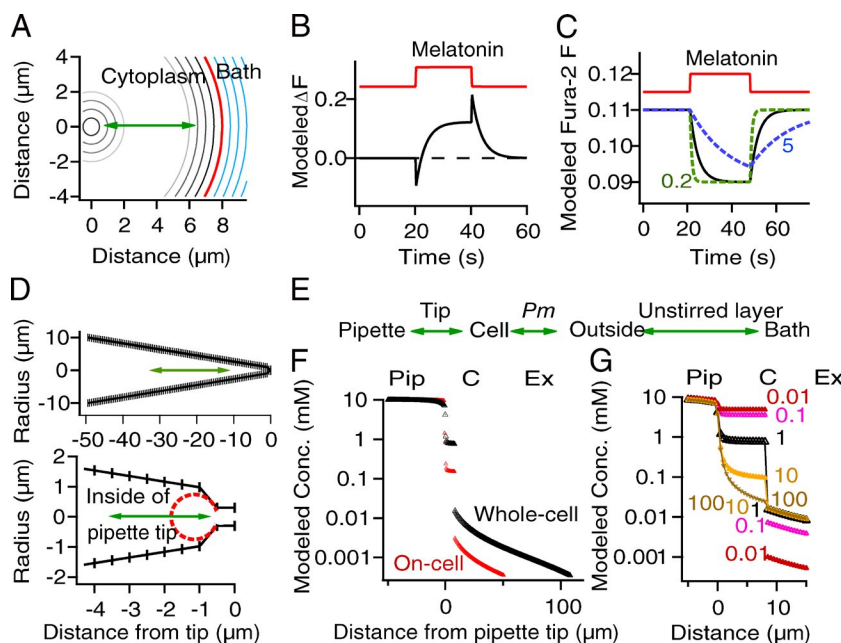
Figure 7. Modeling the permeation experiments. (A) Geometry of the simulated cell and bathing medium. Spherical shells are placed every 0.5 μm from the cell center out for 150 μm. The cell membrane (red) is the boundary between the 16th and 17th shells. The arrow symbolizes diffusion of molecules between shells. (B) Simulation of the experiment in Fig. 4 D showing ΔF, the difference in melatonin fluorescence, with and without cells in the chamber while melatonin was perfused in the bath for 20 s. The axis was rescaled to match the experiment. (C) Simulation of the experiment in Fig. 5 B showing the transient decrease in Fura-2 fluorescence as melatonin is perfused in the bath. The trace is actually the calculated time course of intracellular melatonin rescaled to match the presentation of the experiment. Two dashed traces labeled 5 and 0.2 show the effect of increasing the assumed membrane permeability by 5 or decreasing it to 0.2 times the standard melatonin value. (D) Geometry of the simulated pipette. See section "Adding the pipette." The dashed circle represents the

assumed shape of the Ω-shaped on-cell membrane patch when it was needed. It has an area of 14.7 μm² chosen to match the increase of extracellular amperometric signal upon breaking the patch to go to whole-cell configuration. (E) Schematic of the diffusion regimen in the model simulation. (F) Decay of melatonin concentration with distance in the model. Negative distances are inside the pipette. The pipette, cell, and extracellular domains are marked Pip, C, and Ex, respectively. (G) Decay with distance of molecules of different assumed membrane permeability in the model. Numbers are multipliers, so that that curve marked 10 assumes a membrane permeability of 10× the standard melatonin value of 1.7 μm/s, etc.

before it is in the extracellular space. For pinealocytes, the residence time should be similar because they showed identical amperometric signals in the dialysis experiments. The lifetime in pinealocytes and in other cell types ought to be governed by a similar permeability and would differ only in detail depending on cell surface area and volume. For example, for a cell half as large (8-μm diameter), the surface to volume ratio is double and the time constant for melatonin equilibration would be one half (1.8 s). The high membrane permeability accounts for the reported ability of melatonin to leave multilamellar lipid vesicles in <90 min (Costa et al., 1995) and to be delivered in humans orally, sublingually, intranasally, and by transdermal patch. A daytime transdermal patch containing 2.1 mg melatonin can raise the circulating plasma concentration to equivalent night concentrations of 400–800 pmol/liter in 4 h and prolong daytime sleep (Aeschbach et al., 2009). In rats and humans, intranasally applied melatonin crosses the blood–brain barrier and reaches a maximum in cerebrospinal fluid in 15 min (van den Berg et al., 2004). The octanol partition coefficient of melatonin is almost the same as that of nicotine (Table 2), a compound well known to reach the central nervous system quickly after inhalation.

High permeability has several consequences for experiments. As was shown here, both fast perfusion and fast real-time assays are needed to measure the permeability. Few other studies have achieved these goals for biological membranes with such permeant compounds. For the same reason, it is generally impractical to ask whether such a compound acts on the inside or on the outside of the cell. A highly permeant compound will be on both sides of the membrane at almost equal concentrations whether it is applied inside the cell or outside the cell. This difficulty was apparent, for example, earlier in studies of local anesthetics that have a partition coefficient into lipid an order of magnitude higher than that of melatonin (Table 2, lidocaine). For them it was necessary to have fast flow and also impermeant quaternary derivatives and protonated molecules to ask the sidedness question (Hille, 1977a,b). A tethered ligand might also work. A second consequence applies to measurements of melatonin secretion. Some investigators have measured the pineal gland melatonin content (e.g., Afeche et al. [2006]), and others measure the medium (Yamada et al., 1998). We would suggest that the content of the gland would be a less reliable index than the content of the medium because melatonin might leave the cells and perhaps the gland within seconds, before the measurement could be made. Careful washing of the gland might suffice to deplete all but the newly synthesized melatonin. A final consequence is that melatonin receptors on intracellular compartments will encounter ambient melatonin as readily as receptors on the plasma membrane.

Permeability and leakage of indoleamines and other compounds

We have estimated that the plasma membrane permeability for melatonin is 1.7 μm/s (0.00017 cm/s). What are the permeabilities in living cells for other indoleamines and related compounds in Table 2? These are not yet determined directly, but taking our estimated melatonin permeability and the table of K_{oct}, we have estimated the permeabilities of the neutral species of other compounds by the empirical equation

$$P_m = 0.069 * K_{oct} \; \mu m/s. \tag{1a}$$

This is ∼1,300-fold lower than the permeabilities in lecithin planar bilayers, Eq. 3. These values are plotted as the bottom set of green symbols and dashed line in Fig. 6. For practical use at pH 7.4, the permeability for cells would become

$$P_{cell} = 0.069 * K_{oct} * (\% \; neutral \, / \, 100) \; \mu m/s. \tag{1b}$$

These values are given in Table 2 as P_{cell}. Relative to melatonin, the amperometric concentration outside a dialyzed cell for NAS was 18% and the K_{oct} is 19% (Tables 1 and 2). Neither of the two optical methods worked to give equilibration time constants with the cell for NAS. Thus, our best estimate is that P_{cell} for NAS might be 0.33 μm/s, five times less than that for melatonin. That would lengthen the cell bath equilibration time to ∼18 s for NAS. Microdialysis of the pineal region in a rat reveals that NAS (the immediate precursor of melatonin) is secreted at night on exactly the same schedule as melatonin (Liu and Borjigin, 2006). However, the NAS secretion is strikingly five times greater than the melatonin secretion. Because NAS is synthesized from 5-HT on the way to melatonin (Fig. 1) and because it is membrane permeant, it is inevitable that some of it escapes while the pineal is actively synthesizing melatonin. The microdialysis results suggest that five sixths of the NAS synthesized escapes the pinealocyte before it can be converted into melatonin by the enzyme hydroxyindole-*O*-methyltransferase (HIOMT; Fig. 1).

We turn to 5-HT, catecholamines, and other compounds of lower permeability. It is of considerable physiological interest to know how much they can leak from cells. Once again, we took the measured time constant for equilibration of melatonin across the cell membrane to develop an empirical equation for these molecules at pH 7.4,

$$\tau = 88 \, / \, (K_{oct} * (\% \; neutral \, / \, 100)) \; s, \tag{2}$$

and populated the last column of Table 2 with the results. Nitric oxide, which falls between NAS and 5-HT, is predicted to equilibrate relatively quickly as expected. For 5-HT, the extracellular concentration seen with our amperometry was 0.6% of that for melatonin, or less. The K_{oct} is 13%, but taking into account

Yu et al. 73

its strong protonation (Table 2), the effective octanol distribution becomes only 0.07% of that for melatonin, and the predicted exponential time constant at pH 7.4 is as long as 1.5 h. Indeed, several papers describe activity-dependent and quantal (vesicular) release of 5-HT as might be expected for a less-permeant neurotransmitter packaged in vesicles (e.g., Bruns and Jahn [1995]; Tao et al. [1997]; Adell and Artigas [1998]).

Despite a low effective permeability, a recent paper describes a nonquantal and activity-independent background efflux of 5-HT in the neuropil of the dorsal Raphe nucleus, giving enough extracellular 5-HT to activate local autoreceptors (Mlinar et al., 2015). This seems plausible with the above permeability coefficient if we recognize that the time constants of Eq. 2 are predicted for a 16-µm diameter cell and will shorten inversely with the surface to volume ratio. Consider that in the neuropil the surface to volume ratio of fine processes may be 100 or more times that of a tsA201 cell, i.e., cell processes may be <160 nm in diameter. The 1.5-h cytoplasm bath equilibration time would become 54 s. Thus, a molecule of only modest permeability could transition from exocytotic to diffusional modes depending on surface to volume ratios. Extending this argument might seem to suggest that cytoplasmic 5-HT–containing vesicles would empty quickly back into the cytoplasm; however, their acidic pH, if 2 U below the cytoplasmic pH, would slow such a process by another 100-fold. Judging from their K_{oct} values and fraction uncharged, the catecholamines epinephrine, norepinephrine, and dopamine would fall into a category that is two- to fivefold less permeable than 5-HT (Table 2). They would be very slightly permeant and perhaps capable of leaking from neutral pH cytoplasm when surface to volume ratios are high, but they also can be retained in vesicles because of acidic vesicular pH and also because of complexation with chromogranins, ATP, and other molecules that help retain them (Videen et al., 1992). The larger the vesicle, the more they can be retained. Thus, large dense core vesicles and chromaffin granules will be the most efficient storage.

Conclusion
In summary, melatonin and NAS are highly permeant neutral molecules that will leak out of cells as rapidly as they are synthesized. Like nitric oxide and endo cannabinoids, their secretion is controlled by regulating the rate of synthesis (Simonneaux and Ribelayga, 2003).

APPENDIX

Comparison of indoleamines with other model compounds
As a theoretical attempt to predict membrane permeability, we compare physical properties of indoleamines with those of model compounds. In landmark papers, Finkelstein (1976) and Orbach and Finkelstein (1980) revisited the Overton-Meyer rule, comparing lipid solubility of compounds with their membrane bilayer permeability (see also Walter and Gutknecht [1986]). They reviewed what is called the solubility-diffusion mechanism and presented arguments that the permeability is proportional to the product of the partition coefficient into lipid times the diffusion coefficient in lipid. Because the diffusion coefficient is nearly a constant for molecules like those in Table 2 (Orbach and Finkelstein, 1980), the principal determinant of their permeability is the partition coefficient. In Table 2, compounds are listed in order of increasing n-octanol/water partition coefficient K_{oct}. Octanol was chosen here because it is the preferred comparison solvent for permeation in the pharmaceutical industry, so such data are readily available. Partition coefficients are usually reported as $\log_{10}$ values, conventionally called "log P" in the published tables and in the prediction programs. However, after Orbach and Finkelstein (1980) and to avoid confusing these numbers with P_m, the membrane permeability, we use the less conventional notation here "log K_{oct}" and then translate them to K_{oct} by raising 10 to that power. The log K_{oct} values given in Table 2 are the mean of several theoretical and experimental (where available) values (see legend) but still are only approximate because the values averaged sometimes differed by as much as 1.0 log unit. K_{oct} values of 4.8 and 25 for NAS and melatonin mean that they will be more concentrated in lipid than in water. Partition coefficients always are measured and calculated for the uncharged form of an ionizable molecule. Many of the amine compounds in Table 2 will be mostly protonated at physiological pH, giving them a positive charge and reducing both the partition into lipid and the effective permeability accordingly. Therefore, although the neutral partition coefficient for 5-HT is as high as 3.2, as only 0.5% of 5-HT molecules are neutral at pH 7.4, the predicted 5-HT distribution into octanol falls to 0.016 relative to water (Table 2), vastly smaller than for NAS or melatonin.

Table 2 also gives membrane permeability values for several model compounds measured in different lipid bilayers (Orbach and Finkelstein, 1980). Those plotted as red circles in Fig. 6 correlate with K_{oct} values. The red regression line obeys the formula

$$P_m = 90 * K_{oct} \ \mu m/s. \tag{3}$$

As was explained in the section "Comparison of indoleamines with other model compounds", these permeabilities were measured in planar lipid bilayers made from egg lecithin/hexadecane or phosphatidylcholine/decane. Permeabilities in actual cell membranes are expected to be much lower (by our measurements >1,000-fold lower, c.f. our Eqs. 1a and 1b), but there is no

systematic study that compares "black" lipid planar bilayers with cell membranes. Two arguments for lower values in living cells include (1) that permeabilities measured in "tighter" lecithin-cholesterol, sphingomyelin-cholesterol, or tocopherol/cholesterol/brain lipid planar bilayers are 10- to 1,000-fold smaller than those for lecithin bilayers (Fig. 6, bottom red triangle; Finkelstein, 1976; Walter and Gutknecht, 1986) and (2) that living cells may have 50% proteins in the membrane that form complexes with the lipids, probably leaving only a quite reduced fraction of the membrane lipids free to dissolve permeating molecules. Fig. 6 also plots red crosses for the other physiological compounds in Table 2, including the indoleamines. They are plotted using P_m values from Eq. 3 predicted for lecithin planar bilayers and neutral species. Again, these values should be much higher than those for membranes of living cells.

What do the permeability numbers mean? For a membrane, the flux is the product of the permeability coefficient (P_m), the area (A), and the concentration difference across the membrane (Δc; Danielli, 1941):

$$Flux = -P_m A \Delta c. \tag{4}$$

In physiology the conventional units have been centimeters, seconds, and moles. Here, we use micrometers instead of centimeters. The permeability then would have units of micrometers/second, like a velocity. The meaning is simply illustrated. Consider a planar membrane with solute on only one side at concentration c and permeability P_m. Then in 1 s, the one-way membrane flux per unit area is $P_m c$, exactly as though the solute were moving uniformly at a velocity of P_m µm/s across the membrane. Although it is not really correct, heuristically, one could imagine the solute translating in bulk at this velocity. Thus, to a first approximation, if P_m were 2 µm/s, a spherical cell of radius 8 µm would be emptied in 4 s, and a 100-nm vesicle would be emptied spontaneously in 25 ms. Such a solute would be considered highly membrane permeant and not a candidate for storage in membrane vesicles or a molecule that could be confined within a cell. By these arguments, even if cell membranes were like the tighter sphingomyelin-cholesterol planar bilayers, NAS and melatonin would be in the category of highly permeant compounds.

REFERENCES

Adell, A., and F. Artigas. 1998. A microdialysis study of the in vivo release of 5-HT in the median raphe nucleus of the rat. *Br. J. Pharmacol.* 125:1361–1367. http://dx.doi.org/10.1038/sj.bjp.0702206

Aeschbach, D., B.J. Lockyer, D.J. Dijk, S.W. Lockley, E.S. Nuwayser, L.D. Nichols, and C.A. Czeisler. 2009. Use of transdermal melatonin delivery to improve sleep maintenance during daytime. *Clin. Pharmacol. Ther.* 86:378–382. http://dx.doi.org/10.1038/clpt.2009.109

Afeche, S.C., R. Barbosa, J.H. Scialfa, I.M. Terra, A.C. Cassola, and J. Cipolla-Neto. 2006. Effects of the blockade of high voltage-activated calcium channels on in vitro pineal melatonin synthesis. *Cell Biochem. Funct.* 24:499–505. http://dx.doi.org/10.1002/cbf.1270

Bean, R.C., W.C. Shepherd, and H. Chan. 1968. Permeability of lipid bilayer membranes to organic solutes. *J. Gen. Physiol.* 52:495–508. http://dx.doi.org/10.1085/jgp.52.3.495

Bruns, D., and R. Jahn. 1995. Real-time measurement of transmitter release from single synaptic vesicles. *Nature.* 377:62–65. http://dx.doi.org/10.1038/377062a0

Costa, E.J.X., R.H. Lopes, and M.T. Lamy-Freund. 1995. Permeability of pure lipid bilayers to melatonin. *J. Pineal Res.* 19:123–126. http://dx.doi.org/10.1111/j.1600-079X.1995.tb00180.x

Danielli, J.F. 1941. Cell permeability and diffusion across the oil-water interface. *Transactions of the Faraday Society.* 37:121–124. http://dx.doi.org/10.1039/tf9413700121

Dickson, E.J., B.H. Falkenburger, and B. Hille. 2013. Quantitative properties and receptor reserve of the IP3 and calcium branch of Gq-coupled receptor signaling. *J. Gen. Physiol.* 141:521–535. http://dx.doi.org/10.1085/jgp.201210886

Finkelstein, A. 1976. Water and nonelectrolyte permeability of lipid bilayer membranes. *J. Gen. Physiol.* 68:127–135. http://dx.doi.org/10.1085/jgp.68.2.127

Fushimi, K., and A.S. Verkman. 1991. Low viscosity in the aqueous domain of cell cytoplasm measured by picosecond polarization microfluorimetry. *J. Cell Biol.* 112:719–725. http://dx.doi.org/10.1083/jcb.112.4.719

Gingrich, K.J., P.M. Burkat, and W.A. Roberts. 2009. Pentobarbital produces activation and block of $\alpha_1\beta_2\gamma_{2S}$ GABAA receptors in rapidly perfused whole cells and membrane patches: Divergent results can be explained by pharmacokinetics. *J. Gen. Physiol.* 133:171–188. http://dx.doi.org/10.1085/jgp.200810081

Haidekker, M.A., T.P. Brady, D. Lichlyter, and E.A. Theodorakis. 2005. Effects of solvent polarity and solvent viscosity on the fluorescent properties of molecular rotors and related probes. *Bioorg. Chem.* 33:415–425. http://dx.doi.org/10.1016/j.bioorg.2005.07.005

Hille, B. 1977a. Local anesthetics: hydrophilic and hydrophobic pathways for the drug-receptor reaction. *J. Gen. Physiol.* 69:497–515. http://dx.doi.org/10.1085/jgp.69.4.497

Hille, B. 1977b. The pH-dependent rate of action of local anesthetics on the node of Ranvier. *J. Gen. Physiol.* 69:475–496. http://dx.doi.org/10.1085/jgp.69.4.475

Kim, M.H., S. Uehara, A. Muroyama, B. Hille, Y. Moriyama, and D.S. Koh. 2008. Glutamate transporter-mediated glutamate secretion in the mammalian pineal gland. *J. Neurosci.* 28:10852–10863. http://dx.doi.org/10.1523/JNEUROSCI.0894-08.2008

Koh, D.S., and B. Hille. 1997. Modulation by neurotransmitters of catecholamine secretion from sympathetic ganglion neurons detected by amperometry. *Proc. Natl. Acad. Sci. USA.* 94:1506–1511. http://dx.doi.org/10.1073/pnas.94.4.1506

Koh, D.S., and B. Hille. 1999. Rapid fabrication of plastic-insulated carbon-fiber electrodes for micro-amperometry. *J. Neurosci. Methods.* 88:83–91. http://dx.doi.org/10.1016/S0165-0270(99)00020-5

Law, V., C. Knox, Y. Djoumbou, T. Jewison, A.C. Guo, Y. Liu, A. Maciejewski, D. Arndt, M. Wilson, V. Neveu, et al. 2014. DrugBank 4.0: shedding new light on drug metabolism. *Nucleic Acids Res.* 42:D1091–D1097. http://dx.doi.org/10.1093/nar/gkt1068

Liu, T., and J. Borjigin. 2006. Relationship between nocturnal serotonin surge and melatonin onset in rodent pineal gland. *J. Circadian Rhythms.* 4:12. http://dx.doi.org/10.1186/1740-3391-4-12

Mlinar, B., A. Montalbano, G. Baccini, F. Tatini, R. Berlinguer Palmini, and R. Corradetti. 2015. Nonexocytotic serotonin release tonically suppresses serotonergic neuron activity. *J. Gen. Physiol.* 145:225–251. http://dx.doi.org/10.1085/jgp.201411330

Orbach, E., and A. Finkelstein. 1980. The nonelectrolyte permeability of planar lipid bilayer membranes. *J. Gen. Physiol.* 75:427–436. http://dx.doi.org/10.1085/jgp.75.4.427

Reiter, R.J. 1991. Melatonin: the chemical expression of darkness. *Mol. Cell. Endocrinol.* 79:C153–C158. http://dx.doi.org/10.1016/0303-7207(91)90087-9

Rice, M.E., G.A. Gerhardt, P.M. Hierl, G. Nagy, and R.N. Adams. 1985. Diffusion coefficients of neurotransmitters and their metabolites in brain extracellular fluid space. *Neuroscience.* 15:891–902. http://dx.doi.org/10.1016/0306-4522(85)90087-9

Sangster, J. 1989. Octanol-water partition coefficients of simple organic compounds. *J. Phys. Chem. Ref. Data.* 18:1111–1229. http://dx.doi.org/10.1063/1.555833

Sharma, A., and S.G. Schulman. 1999. Introduction to Fluorescence Spectroscopy. John Wiley and Sons, Inc., New York. 192 pp.

Shida, C.S., A.M. Castrucci, and M.T. Lamy-Freund. 1994. High melatonin solubility in aqueous medium. *J. Pineal Res.* 16:198–201. http://dx.doi.org/10.1111/j.1600-079X.1994.tb00102.x

Simonneaux, V., and C. Ribelayga. 2003. Generation of the melatonin endocrine message in mammals: a review of the complex regulation of melatonin synthesis by norepinephrine, peptides, and other pineal transmitters. *Pharmacol. Rev.* 55:325–395. http://dx.doi.org/10.1124/pr.55.2.2

Tao, R., Z. Ma, and S.B. Auerbach. 1997. Influence of AMPA/kainate receptors on extracellular 5-hydroxytryptamine in rat midbrain raphe and forebrain. *Br. J. Pharmacol.* 121:1707–1715. http://dx.doi.org/10.1038/sj.bjp.0701292

van den Berg, M.P., P. Merkus, S.G. Romeijn, J.C. Verhoef, and F.W. Merkus. 2004. Uptake of melatonin into the cerebrospinal fluid after nasal and intravenous delivery: studies in rats and comparison with a human study. *Pharm. Res.* 21:799–802. http://dx.doi.org/10.1023/B:PHAM.0000026431.55383.69

Videen, J.S., M.S. Mezger, Y.M. Chang, and D.T. O'Connor. 1992. Calcium and catecholamine interactions with adrenal chromogranins. Comparison of driving forces in binding and aggregation. *J. Biol. Chem.* 267:3066–3073.

Walter, A., and J. Gutknecht. 1986. Permeability of small nonelectrolytes through lipid bilayer membranes. *J. Membr. Biol.* 90:207–217. http://dx.doi.org/10.1007/BF01870127

Yamada, H., S. Yatsushiro, S. Ishio, M. Hayashi, T. Nishi, A. Yamamoto, M. Futai, A. Yamaguchi, and Y. Moriyama. 1998. Metabotropic glutamate receptors negatively regulate melatonin synthesis in rat pinealocytes. *J. Neurosci.* 18:2056–2062.

Yu, H., J.B. Seo, S.R. Jung, D.S. Koh, and B. Hille. 2015. Noradrenaline upregulates T-type calcium channels in rat pinealocytes. *J. Physiol.* 593:887–904. http://dx.doi.org/10.1113/jphysiol.2014.284208